Journal of Nanophotonics

SPIEDigitalLibrary.org/jnp

Synthesis, electromechanical characterization, and applications of graphene nanostructures

Traian Dumitrică
Suneel Kodambaka
Sukky Jun

SPIE

Synthesis, electromechanical characterization, and applications of graphene nanostructures

Traian Dumitrică,[a] Suneel Kodambaka,[b] and Sukky Jun[c]
[a]University of Minnesota, Department of Mechanical Engineering, Minneapolis, Minnesota 55455
E-mail: td@me.umn.edu
[b]University of California Los Angeles, Department of Materials Science and Engineering, Los Angeles, California 90095
[c]University of Wyoming, Department of Mechanical Engineering, Laramie, Wyoming 82071

Abstract. The emerging field of graphene brings together scientists and engineers as the discovered fundamental properties and effects encountered in this new material can be rapidly exploited for practical applications. There is potential for a two-dimensional graphene-based technology and recent works have already demonstrated the utility of graphene in building nanoelectromechanical systems, complex electronic circuits, photodetectors and ultrafast lasers. The state-of-the-art of substrate-suported graphene growth, and the current fundamental understanding of the electromechanical properties of graphene and graphene nanoribbons, represent important knowledge for developing new applications. © *2012 Society of Photo-Optical Instrumentation Engineers (SPIE).* [DOI: 10.1117/1.JNP.6.064501]

Keywords: graphene; nanoribbons; growth; electromechanical properties.

Paper 11094V received Sep. 12, 2011; revised manuscript received Nov. 27, 2011; accepted for publication Nov. 28, 2011; published online Feb. 24, 2012; corrected Mar. 19, 2012.

1 Introduction and Overview of Applications

The discovery of graphene[1]—a single-layer of carbon atoms covalently bonded in a two-dimensional hexagonal lattice—has drawn tremendous attention for many areas of fundamental and applied research. Graphene presents a combination of extraordinary material properties, such as high charge carrier mobility ($\sim 200,000$ cm^2 V/s),[2] tunable optical properties,[3] tunable band gap,[4] flexibility and high Young's modulus (1,100 GPa),[5] robustness and environmental stability, and high thermal conductivity ($\sim 5,000$ W/mK).[6] Exploiting such properties may enable ground-breaking applications in electronic,[7] including thermal management of nano-electronics, bio[8] and photonic devices,[9–11] novel nanoelectromechanical applications,[12] and composite materials.[13,14]

The rich properties of graphene largely arises because of two important aspects: the strength of the bonds that keeps the carbon atoms together and the peculiar electronic structure of the honeycomb lattice. The outstanding mechanical properties, which originate in the sp^2 hexagonal backbone, are attracting more and more mechanical engineers, and the effort is paying off. Recently, electromechanical resonators fabricated from graphene sheets have been reported.[15] The thinnest resonator built using a mono-layer graphene represents the ultimate limit of two-dimensional nanoelectromechanical systems. Graphene has also been integrated in complex microfabricated structures to create a new class of membrane-based devices impermeable to standard gas species, including helium.[16]

Graphene's fascinating electronic properties, such as being a semi-metal yet optically transparent, are a direct consequence of the delocalized π orbital structure, which gives rise to a unique electronic band structure. The fundamental aspects of the electronic states in graphene have been the focus of many excellent reviews, including Ref. 17, and therefore will not be repeated here. The conduction band and the valence band energies are in contact only at discrete points within the hexagonal Brillouin zone. Zooming near this **K** point, the energy dispersion is

0091-3286/2012/$25.00 © 2012 SPIE

linear rather than the expected quadratic in the electronic wavevector $|\mathbf{k}|$. This linear dispersion relationship defines two cones in $\mathbf{k}$ space whose vertices meet at the $\mathbf{K}$ point. Opening a band gap in graphene is one of the most important research topic. A number of approaches have been implemented, such as the application of an uniaxial strain,[18] by cutting graphene into nanoribbons and quantum dots.

Different, but similarly fascinating, properties are exhibited by double-, few- and multi-layer graphene. Consider the electrical domain. The electronic excitations of the mono-layer are described using the Dirac equation, a modified version of the Schrödinger equation that includes the effects of special relativity. Such a treatment gives rise to new quasiparticles, the massless Dirac fermions, which are the charge carriers in graphene. The massless Dirac spectrum of electrons in a single-layer graphene has been thoroughly studied, both theoretically and experimentally.[17] There are dramatic changes in the electronic properties in a few-layer graphene as compared with mono-layer graphene.[19] When two or more layers of graphene are present, the characteristic linearly dispersing bands of the single-layer are either replaced or augmented by pairs of split-hyperbolic bands. These new bands correspond to fermions of finite mass.[20]

The electronic properties of graphene have opened new possibilities for reengineering electronic components and circuitry with higher performances. This is a new and rapidly growing field, where the device architecture has evolved from simple to complex circuitry within a short time span. To-date, a high-frequency (>300 GHz) graphene-based transistor[21] has already been demonstrated. A complex graphene circuit [22] was demonstrated in which all circuit components, including graphene field-effect transistors and inductors, were integrated on a single silicon carbide wafer. The integrated circuit operates as a broadband radio-frequency mixer at frequencies up to 10 GHz.

Even in the absence of a band gap, graphene shows remarkable optical properties that makes it very promising for photonic and optoelectronic applications,[9] including transparent conductors, photovoltaic cells, light-emitting devices, saturable absorbers, and lasers.[11] For example, the linear dispersion of the Dirac electrons makes broadband applications possible. Graphene could also be made luminescent.[23,24] In another case, a graphene photodetector was demonstrated,[10] which can accurately detect optical data streams at speed of 10 Gbit/s, a figure that compares well to the currently used optical detectors made of group III-V semiconductors.

The general topic graphene has attracted so much attention that, according to the ISI Web of Science, over 240 review articles have been published on the topic "graphene" since 2004, with nearly 90 reviews published in 2010 alone. We realize that summarizing this amount of literature (and with more articles being published daily) is a daunting task. Instead of attempting to present an exhaustive overview on this topic, we focus our efforts on three areas, which present great interest for advancing applications.

Efficient *growth of graphene* samples that can be used to investigate the fundamental characteristics and build devices represents an outstanding current problem. In Sec. 2 we focus on promising substrate-supported growth approaches. These methodologies represent a route for graphene integration into devices by deterministic placement in a pre-defined position on a substrate of choice. Alternatively, the substrate-grown graphene flakes can be subsequently transferred to a desired location. A number of techniques to fabricate graphene nanoribbons are briefly reviewed. For those interested in the related topics, such as synthesis of functionalized graphene, graphane (hydrogenated graphene), graphene oxide and other graphitic materials, please see Refs. 25–28 and references therein.

Understanding the fundamentals underlying the behavior of graphene is required to envisage new applications and to design, model, simulate, fabricate, and control novel nanodevices. Scaling a device down to the micro- and nano-scale often comes with unique complications and limitations that must be resolved in advance of manufacturing. Theory and computation are key enablers in reaching these goals. In Sec. 3 we are concerned with *mechanical properties* of graphene from a microscopic perspective. We discuss various experimental situations in which the relations of macroscopic elasticity can be used, without the need of microscopic modeling. *Graphene nanoribbons* are new one-dimensional materials derived from graphene and are important because taking advantage of the lateral quantum confinement provides a route for band gap opening. Their structural and electronic properties exhibit a combination of surface and edge characteristics. What distinguishes them from the widely studied single-wall, seamless carbon

nanotubes, are the edge characteristics. In Sec. 4, we review the physical properties of graphene nanoribbons and their edges. Particular emphasis is placed on elastic stability, deformation behavior, and the modification of electronic properties induced by mechanical strain.

2 Growth of Graphene Samples

Graphene has most commonly been synthesized via mechanical or chemical exfoliation of individual layers from bulk graphite, thermal carburization of single-crystalline SiC surfaces, deposition of carbon from solid sources or vapor precursors onto single- as well as poly crystalline substrates, surface segregation of carbon dissolved in the bulk of a metal, and metal-catalyzed recrystallization of amorphous carbon. A review of all these synthesis methods along with recent developments in the chemical vapor deposition (CVD) of graphene can be found in Ref. 29

2.1 *Free-Standing Graphene*

The surge in research activities on graphene could probably be attributed to one simple technique—mechanical exfoliation from bulk graphite, which involves the physical cleaving of single and/or few-layer graphene from highly oriented pyrolytic graphite (HOPG).[30] This method, also referred to as "the scotch tape technique" has, by far, yielded the best charge carrier mobilities.[31] From the exfoliated graphene sheets, nano-scale ribbons have been fabricated using lithography as a means to controllably tune the band gap of graphene.[32–35] Recently, this method has been extended to prepare "graphene nanomesh" of desired size and periodicity using block copolymer lithography.[36] Reviews on the patterning of graphene nanostructures can be found in Refs. 37 and 38 Highly regular nanoribbons have also been synthesized using a wet chemical process that yields functionalized graphene.[39] Additional details on wet chemical methods to produce graphene can be found in Refs. 40 and 41.

Graphene layers can be extracted from bulk graphite via chemical intercalation. In this approach, large metal atoms such as Na, Li, or K help break the van der Waals bonding between the graphene sheets. Typically this is carried out by heating a powder mixture of graphite and the metal in an inert atmosphere.[42] More recently, Zn was used to controllably remove graphene layer-by-layer from the substrates in a controlled manner.[43] Graphene sheets can also be synthesized via intercalation of Ge into graphitized SiC.[44] This method may be more suitable for large-scale preparation of crystalline graphene sheets via exfoliation directly on semiconducting surfaces.

Following the discovery of free-standing graphene, researchers focused their attention on the epitaxial and large-scale growth of graphene on substrates. In the following sections, we give an overview of the research directed on two approaches, graphene growth on SiC(0001) and on metal surfaces, that have gained significant momentum recently.

2.2 *Graphene Grown on SiC(0001)*

One of the popular methods to produce graphene sheets is via thermal carburization of SiC (0001). This process, observed at least four decades ago,[45] has recently received considerable attention. This is because crystalline graphene layers can be grown directly on semiconducting or insulating wafers despite the large lattice mismatch (~19%).[46–49] Another attractive feature of this approach is that conventional lithography and other processes, compatible with existing microelectronics technology, can be used for the large-scale fabrication of graphene-based devices directly on SiC and even on Si wafers.[50–53]

In this process, single-crystalline SiC(0001) substrates are heated to high temperatures (greater than 1000 °C) in ultrahigh vacuum (UHV) or inert atmospheres. During annealing, silicon atoms preferentially desorb from the surface, leaving behind a carbon-rich surface. With increasing annealing temperature and time, a series of surface reconstructions are observed as the surface becomes progressively richer in carbon and eventually graphene is formed. The distinct feature in the synthesis of graphene on SiC is the existence of an intermediate Si-deficient (or C-rich) layer (also referred to as the buffer layer), which exhibits a $(6\sqrt{3} \times 6\sqrt{3})$

reconstruction. This surface, although geometrically similar to that of graphene, is strongly bound to the underlying substrate and does not exhibit any of the electronic characteristics of graphene. Upon further annealing, graphene layer forms on top of this buffer layer. Recent studies have shown that this buffer layer can be decoupled from the substrate by annealing in the presence of oxygen or hydrogen.[54,55]

Studies have shown that surface morphology, crystallinity, graphene layer thickness, and transport characteristics are found to depend on the SiC(0001) substrate surface termination (Si vs C) SiC(0001).[56] For example, multi-layer graphene can be easily grown at relatively lower temperatures on C-terminated SiC(0001) surfaces compared to Si-terminated surfaces.[45] However, the Si-terminated surfaces yield better controllability over layer thickness. For more details, concerning the current status on the role of substrate surface termination on graphene growth-related aspects, please see the following reviews.[57,58]

One of the primary challenges associated with the synthesis of graphene on SiC has been the large-scale uniformity of layer thickness. This is because approximately 3.14 layers of SiC are required to form one mono-layer of graphene and nucleation and growth of graphene depend on the annealing ambient and the SiC surface step structure. For example, in situ low-energy electron microscopy (LEEM) observations have provided valuable insights into the mechanisms underlying the nucleation and growth of graphene on SiC surfaces.[59–64] It is found that annealing the SiC samples in UHV favors heterogeneous nucleation of graphene at the step edges. Since surface and sub-surface carbon atom diffusivities are rather low, high temperatures are required for the formation of smoother films. However, increasing the temperature leads to a higher rate of desorption of Si, which results in localized pits on the substrate. As a consequence, rough surfaces and multi-layered graphene films are produced. In order to overcome this problem, two different methods have been successfully implemented. In one approach, high pressures of argon are used as a means to suppress Si desorption.[65] In the second approach, annealing is carried out in the presence of Si containing gas, which helps increase the Si concentration in the vapor phase and hence suppresses Si desorption.[65] In both these processes, Si desorption is shifted to temperatures higher than those nominally used in vacuum annealing. As a result, carbon atom diffusion is enhanced and leads to smoother graphene films. Variations in the quality of graphene and characteristics of devices fabricated in different laboratories can be attributed to the different processing conditions employed during graphene growth. Therefore, annealing ambient is an important factor controlling the growth of graphene on SiC(0001). More details concerning the role of residual gas chemistry on graphene synthesis can be found in Ref. 66.

2.3 *Graphene Grown on Metals*

Graphene films of desired thicknesses have been grown on single- as well as poly- crystalline metal surfaces using at least three different approaches: controlled precipitation of bulk-dissolved carbon, physical and chemical vapor phase deposition of carbon using solid and gaseous precursors, and solid-state diffusion of carbon.[67–70] Observation of graphene on metal surfaces dates back to the 1970s when researchers were primarily interested in the removal of carbon from the bulk of metals such as Ni, Pt, Pd, and Co.[71–73] UHV annealing experiments involving heat-cool cycles revealed the change in surface carbon concentration with annealing temperature; low-energy electron diffraction (LEED) patterns indicated the presence of crystalline graphitic structure. A variation of this process involves the deposition of carbon onto metal surfaces at elevated temperatures followed by cooling to obtain graphene. Studies have shown that graphene layers can be grown on metals,[74–77] transition-metal carbides (for example, TiC, TaC, WC),[78–80] LaB^6 (100),[81] and hexagonal BN surfaces.[82] A comprehensive summary of all these growth experiments, characterization techniques, and the graphene-substrate interactions can be found in Ref. 83 These approaches received renewed interest in the recent years and graphene films have been grown on a variety of metals including Au, Cu, Ir, Ni, Pd, Pt, Pt-Rh, and Ru.[84–96] For the growth of graphene on metals using any of these approaches, factors such as bulk solubility, rate of cooling, annealing temperature and time, can influence the graphene layer thickness, surface morphology, and in-plane crystallinity.

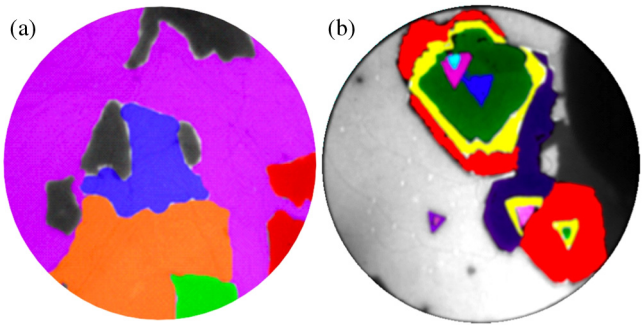

Fig. 1 False-colored low-energy electron microscopy (LEEM) images (field of view is 9.3 μm) of (A) mono-layer and (B) multi-layer graphene-covered Pd(111) samples acquired during annealing at ~790 °C and ~660 °C, respectively in ultra-high vacuum. Each of the colors represents a rotational domain. Incident electron energies used for image acquisition are 17.7 eV and 4.3 eV in A and B, respectively. Mono-layer graphene in A is formed by cooling a carbon-containing Pd(111) sample from ~900 °C to ~790 °C at the rate of 1 K/s, adapted from Ref. 97 The multi-layer graphene in B is obtained by sequential cooling of a Pd(111) sample from ~900 °C to ~790 °C and then to ~660 °C. (unpublished).

For example, Fig. 1 shows LEEM images of mono-layer and multi-layered graphene on Pd (111) grown via segregation from the bulk. Each of the colors represents a rotational domain within (in the case of the mono-layer) and across (for multi-layer) the graphene layers. These domains are a direct consequence of the growth kinetics.

In situ LEEM experiments carried out during carbon deposition on metals helped identify the kinetic and thermodynamic factors controlling graphene growth, the development of rotational domains, and the etching of graphene.[88,98–105] Among all of the metals used so far to grow graphene, Cu proved to be the material of choice due primarily to two seminal studies that showed that large-area, few-layer, graphene can be produced on poly crystalline thin films or foils with potential applications as transparent electrodes in optoelectronic devices.[106,107] These results generated a lot of interest in the last two years and for those interested in learning more about the the current status on this topic, please see Ref. 108.

2.4 *Fabrication of Graphene Nanoribbons*

Motivated by the possibility of tuning electronic and optic properties through quantum confinement, various graphene nanoribbons fabrication methodologies have been pursued. Datta et al.[109] demonstrated a lithographic method by which few-layer graphene samples can be etched along crystallographic axes by thermally activated metallic nanoparticles. They succeeded in etching μm-long crystallographic edges, making the process potentially useful for atomically precise graphene device fabrication. Li et al.[110] developed a solution-phase-derived chemical route to produce graphene nanoribbons with a width below 10 nm, as well as single ribbons with varying widths. The fabricated ribbons exhibited ultrasmooth and well-defined zigzag or armchair edge structures and behave as semiconductors. Jiao et al. demonstrated fabrication approaches by unzipping multiwalled carbon nanotubes by plasma etching[111] and mechanical sonication.[112] These nanoribbons have smooth edges and a narrow width distribution (10 to 20 nm). Most recently, Khlobystov et al.[113] have grown narrow graphene ribbons inside carbon nanotubes. The ribbons are formed via electron irradiation of functionalized fullerenes located inside the tubes. The role of the nanotube is to confine propagation of the nanoribbon in one dimension and determines its width. Therefore, this development appears to establish a much needed reliable method to produce nanoribbons with desirable nanometer scale width. Interestingly, the nanoribbons grown by this method are not flat but helically twisted.

2.5 *Outlook*

There are inherent advantages as well as limitations associated with the growth of substrate-supported graphene. Probably, the most attractive features of using SiC is that it is a wide

band gap material, commonly used as a substrate for the growth of group III-V compound semiconductors, and is compatible with the existing microelectronics processing methods. These attributes facilitate direct fabrication of graphene-based devices. Some of the challenges involved in this process are: the use of extremely high temperatures, the availability of high-quality defect-free substrates, the presence of substrate-induced interactions that affect the transport characteristics, and the lack of a semiconducting bandgap. However, recent studies suggest the possibility of opening up the gap in graphene on SiC by using bilayers, dopants, and an electric field.

In case of graphene on metals, CVD is a promising method especially when metals with limited bulk solubility (such as copper) are used. This is because the CVD process is inherently self-limiting, i.e. graphene grows preferentially on bare metal surfaces rather than on graphene-covered surfaces. As a result, mono-layer graphene can be relatively easily obtained. Hence, CVD process enables the growth of highly uniform graphene layers over large areas even on poly crystalline films. This aspect is attractive for industrial-scale production of graphene especially for transparent conductor applications. For the use of graphene as an active layer in transistors, however, the layers have to be transferred onto non-conducting substrates. This process can damage the layer and limit the device performance.

The substrate-supported graphene can offer additional benefits. For example, studies have shown that the substrate-graphene interactions can alter the electron structure of graphene to the extent that its work function can increase or decrease (with respect to the free-standing layer) and can even behave as a semiconductor. Graphene deposited on substrates often exhibit rotational domains, which are known to affect its transport characteristics. These results are crucial to understanding the behavior of graphene-metal contacts and more studies are desirable. One can also take advantage of the domain-orientation-dependent interactions with the substrate to tailor the properties of graphene layers and graphene-metal contacts. Also, the use of hexagonal boron nitride (hBN) as an epitaxial dielectric layer appears to be promising for the fabrication of graphene-based devices. Finally, graphene/hBN bilayers and sandwich structures may offer interesting possibilities for new applications.

3 Mechanical Properties of Graphene: Theory and Experiment

Recent nanoindentation experiments established the graphene mono-layer as the strongest material ever measured.[5] The outstanding mechanical properties, such as Young's modulus of 1.1 TPa and 130 GPa breaking strength,[5] make this material extremely attractive for many areas of innovation, ranging from nanomanufacturing of various graphene architectures,[114–121] to the use of graphene as reinforcement in composites,[13,14] impermeable atomic membranes,[16] switches and in mass- and force-detection devices that rely on the electromechanics of the out-of-plane deformations.[15,122–126] To pave the way toward applications, it is important to establish the applicability of classical mechanics concepts in quasi-two dimensions. It should be noted that this issue is of great scientific importance. It was the subject of debate[127] in the area of carbon nanotubes, where a Young's modulus value of 5.5 TPa associated with this material caused controversy.

Because the carbon atoms are disposed in a geometric structure that closely resembles the basal planes of bulk graphite, the in-plane elastic properties of graphene can be inferred from the well-studied[5,128] graphite form. However, because of the discreteness in the number of layers N, the out-of-plane deformation modes, such as bending, are of a new nanomechanical nature. Plate, shell, and membrane models are often used for practical investigations of ultrathin graphene layers[123,126–132] The well-studied bulk graphite[128] offers well-defined parameterizations for the continuum plate idealization of a free-standing N-layer graphene: a Young's modulus Y of 1.1 TPa and a thickness of $h = NZ_0$, where $Z_0 = 3.35$ Å is the interlayer distance. One important question addressed here is how many graphene layers are needed before the structure exhibits this plate behavior? Another important aspect is that theoretical modeling usually assumes that the graphene layers are free-standing. However, the experimental studies are mostly carried out using either suspended[16,122,123,126,133,134] or substrate-supported[135,136] graphene. Hence, we will also focus the discussion on relating the theoretical modeling with the behavior indicated by experiments.

3.1 *Microscopic Modeling*

To understand the validity of the plate idealization it is instructive to revisit the tight-binding description of bending recently proposed by Zhang et al.[137] We begin with the well-known partitioning of the wavefunction of hexagonal planar graphene in terms of orthogonal sp^2 hybrids pointing toward the nearest-neighbors, as well as p_z orbitals oriented perpendicular to the plane. Physically, the strong σ bonds formed by the overlap of the nearest neighboring sp^2 hybrids are responsible for the high cohesive energy of graphite and its high in-plane stiffness. The weak π-state bonds formed by the p_z orbitals, sometimes referred to as non-bonding,[138] couple instead to the planar shape.

One important local geometric effect occurring under a pure bending distortion of the mono-layer is that each carbon atom and its three nearest-neighbors are no longer planar but located in the corners of a pyramid. This distortion causes a shift in the sp^2 hybridization. The shift can be incorporated into the planar orbital model using the π-orbital axis vector (POAV) construction introduced by Haddon[139–141] to understand strain in carbon fullerenes. In POAV, the geometrical tilting of σ_i-bonds $(i = 1, 2, 3)$ by an angle θ, Fig. 2, is accomplished by mixing a small degree of s-orbital with the p_z orbitals, generating h_π hybrids. The other important effect caused by the curvature is misalignments between neighboring h_π hybrids.

The tight-binding analysis for the bending strain energy[137] indicates that the strain in the bent mono-layer can be largely captured into the torsional misalignment between the neighboring POAVs. This makes it clear that the mono-layer does not behave as a plate since it exhibits a pure bending curvature without stretching and/or compressing the strong σ network. The second derivative of the bending energy (per atom) with curvature is only 1.6 eV, according to density-functional theory-based calculations.[137]

Bending of the multi-layered graphene was recently addressed by objective molecular dynamics[142,143,144] simulations. Figure 3 illustrates the obtained bending response of the bonds oriented along the principal curvature direction, on which the bending load is transferred most effectively. For multi-layers, there is a splitting with N, indicating that the bent N-layer is stretched at some points and compressed at others, in agreement with the plate phenomenology. Such calculations showed that the bending energy E_b maintains a quadratic dependence on $1/R$ for all N. In bent few-layer graphene, the main source of strain is instead the extension and compression of the constituent layers, confirming the σ-bond origin of strain even in the bent bilayer. Without interlayer sliding, the flexible rigidities follow an N^3 scaling. Some computed values are given in Table 1.

For an N-layered graphene, the resulting h and Y values of the plate model are

$$h = Z_0 N\sqrt{1-\frac{1}{N^2}} \quad \text{and} \quad Y = \frac{CN}{h}. \tag{1}$$

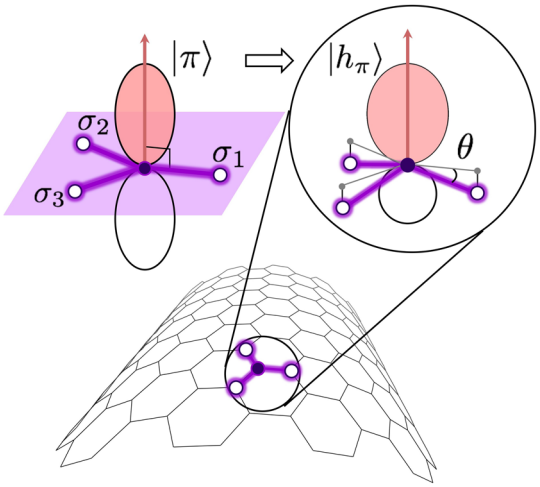

Fig. 2 Diagram showing the π-orbital in planar graphene and its change into h_π when the sheet is bent. The plane delineated by the σ_i bonds was hatched. (Adapted from Ref. 137).

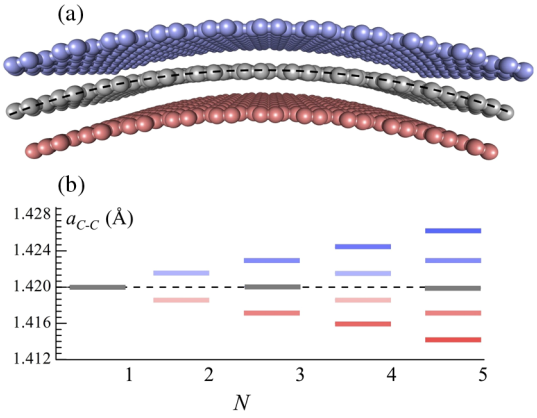

Fig. 3 (a) An $N = 3$ graphene bent with $1/R = 0.15$ nm^{-1}, as obtained by objective molecular dynamics simulations. Dashed line indicates the neutral surface. (a) Length distribution of the carbon-carbon bonds oriented along the principal curvature. (Adapted from Ref. 137).

Table 1 Flexible rigidity D of N-layered graphene,[137] computed from density-functional-based tight-binding (second column).[145] Based on these D values, the last two columns show the resulting plate model.[137]

N	D (eV)	Y (TPa)	h/N (Å)
2	162.70	1.40	2.98
3	660.32	1.27	3.26
4	1589.11	1.26	3.29
5	3206.73	1.24	3.31

This result clearly expresses the role played by the discreteness N. With a quantified $1/2N^2$ error, the N-layered graphene behaves like a continuum nanoplate parameterized by a physically meaningful C/Z_0 Young's modulus and a hZ_0 thickness. Interestingly, each mono-layer component now behaves as a membrane parameterized by C/Z_0 Young's modulus and Z_0 thickness.

3.2 *Mechanical Testing of Ultrathin Graphene*

The above theoretical insights reflect into the various experiments conducted on graphene. In the free-standing mono-layer, the lack of σ-bond participation indicates the breakdown of the plate phenomenology. This result has implications for a broad class of phenomena, where the graphene mono-layer bubbles,[117] folds into a grafold,[118] scrolls its edges,[119] and ripples[134] in spite of its enormous stiffness. These shapes may also induce new and distinct properties. For example, a recent theoretical study indicated that double folding modifies the electronic band structure of graphene.[118] In multi-layer, the vdW forces are mediating the load transfer between layers and bending involves extension or compression of the σ bonds. The plate phenomenology is now fulfilled.

Differences between the mono-layer and multi-layer have indeed been observed in experiments. For example, thorough analyses of elastic properties carried out in connection with bending and vibration tests also indicated that in contrast with the mono-layer, the few-layer graphene is much more rigid against bending.[122,123] Poot and van der Zant[122] performed atomic force microscopy measurements of the mechanical properties of few-layer graphene suspended over circular holes. They found that the plate behavior and the N^3 scaling of the flexural rigidity holds very well up to 10 nm in thickness. This indicates the absence of interlayer sliding and stacking faults in thin graphene samples, thus confirming the plate behavior.

Garcia-Sanchez et al.[123] studied the vibration of suspended few-layer graphene at radio-frequency voltages. The elastic plate theory was applicable in the measured resonators except in those samples storing large nonuniform stresses. Chen et al.[126] demonstrated the fabrication and electrical readout of mono-layer graphene resonators. The dependence of the resonant frequencies follow a squared instead of the plate inverse-quadratic scaling with the mono-layer length. As a result, a continuum membrane is suitable for modeling the suspended mono-layer.

An interesting class of experiments[135,136] involved bending of a cantilever beam made up of a polymer embedded with mono-layer graphene flakes. Such tests revealed remarkable insights into the behavior of these flakes under both tension and compression. It has also been noted that the effect of the lateral support provided by the polymer matrix increases the effective flexural rigidity of graphene by several orders of magnitude. This is a signature of the good mechanical coupling between the graphene flakes and the ploymeric material. Moreover, it was reported that graphene embedded in plastic beams exhibit compression Euler buckling strains, typical for the continuum. The critical strain values of the embedded graphene flakes appear remarkably high compared to those estimated for the suspended ones based on the plate model discussed above. Moreover, at a certain strain the interface between graphene and polymer weakens and fails. A post-mortem examination of these detached flakes identified the presence of permanent wrinkles, in agreement with the breakdown of the plate model in the free mono-layer.

4 Graphene Nanoribbons

In reality, graphene specimen is not an infinitely extended sheet, but a finite-size structure. Ribbons and patches are among structured graphene monolayers that have been studied extensively. The common characteristic of such finite 2 dimensional graphene nanostructures is the presence of edge, which can be considered as a line defect where the domain of hexagonal carbon network is terminated and exposed to the environment. Depending upon their atomic structures, graphene edges are usually classified into zigzag, armchair, combined, and reconstructed types. Physical properties of finite-size graphene nanostructures are often determined by properties of the edge itself, and may substantially differ from those of perfect graphene sheet. A well-known example is the edge state found in graphene nanoribbons, but absent in perfect graphene mono-layer.[146]

4.1 *Edge Stress of Graphene Nanoribbons*

The key physical variables that quantify the stability of surfaces in 3 dimensional crystals are surface energy and surface stress. Surface energy is the excess energy cost to create a new surface, and surface stress refers to the energy to deform a surface.[147] Surface energy provides information about the chemical stability of a surface considered, while we can understand the elastic stability and fundamental deformation behavior of a surface from surface stress. Surface is a planar defect of 3-D crystal and edge is a line defect of 2-D atomic crystal. Noting this analogy, edge energy is defined as the energy cost to create a new edge in a 2-D crystalline material. Edge energy is equivalent to the edge formation energy and has been calculated by many researchers for graphene nanoribbons. However, it is relatively recent that edge stress was introduced along this line of edge excess variables.

Jun[148] defined edge stress of 2-D crystals as the energy cost to stretch an edge along the edge direction and, using first-principles calculations based on density-functional theory, found that pristine armchair and zigzag edges of graphene nanoribbons are both in compressive stress state. Edge stresses of hydrogen-passivated graphene edges were also calculated and found to be negligibly small, which implies that hydrogen passivation stabilizes the dangling bond of edge atoms and prevents the edges from severe elastic deformation.

Shenoy et al.[120] independently calculated the edge stresses of armchair and zigzag graphene nanoribbons using empirical molecular dynamics and obtained the same compressive edge states. A compressive edge stress means that the lower energy state of edge is the one stretched. Therefore, if we set them free to deform, graphene edges tend to stretch the edge length by rippling deformation. Shenoy et al.[120] showed that this rippling behavior is the intrinsic property

of graphene nanoribbon edges, not the temperature effect, and its origin is the compressive edge stress. They incorporated edge stress values into continuum-based energetics and reproduced twisting, scrolling, and rippling behaviors of graphene sheets and ribbons through continuum finite element simulations. For nanoribbons, the influence of edge stress is so substantial that it leads to large-scale twisting deformation.

Huang et al.[149] furthered the study of graphene edge stress by first-principles calculations and found several interesting quantum effects in relation to edge stresses. First, they found that values of armchair edge stress oscillate by a period of three with respect to ribbon width. Similar threefold oscillation has previously been found for the energy gap of armchair graphene nanoribbons, and explained in terms of topological analysis of the hexagonal atomic structure of armchair nanoribbons by Son et al.[150] This connection between energy gap and edge stress is a clear evidence of the electronic origin of edge stress, although their threefold oscillations are out of phase from each other. Fig. 4 shows the width-dependent patterns of edge energy and edge stress armchair graphene nanoribbons. Data was obtained by first-principles calculations based on the density-functional theory with local density approximation and pseudopotentials. Huang et al.[149] also showed that the edge magnetization of zigzag graphene nanoribbon reduces edge stress, leading to more stable and flat zigzag edges. This finding is significant because spin polarization and mechanical properties can affect mutually, i.e., not just strain-induced magnetization or de-magnetization. They also showed that the hydrogen passivation and the Stone-Wales reconstruction of edges can improve the chemical and elastic stabilities of planar graphene edges by lowering the edge energy and by converting edge stress from compression to tension.

Graphene edge can also be viewed as a boundary line that separates graphene domain and vacuum region. Recently, it has been shown that graphene can form a boundary line with edges of boron nitride monolayers[151] and poly crystalline graphenes are made of graphene grains separated by lines of grain boundaries.[152] Chemical hybridizations of graphene and boron nitride monolayers have previously been investigated such as doping of B and N atoms on graphene and replacement of carbon atom in graphene by B and N atoms. However, this domain hybridization by Ci et al.[151] is unique because the two domains are structurally patched to result in nanostructured composite materials by 2-D atomic crystal monolayers.

By using first-principles calculations, Pruneda[153] studied the electronic properties of heterophase superlattices consisting of graphene and boron nitride stripes. It was shown that the superlattices are semiconducting or semi-half-metallic depending upon the width of stripes and the atomic structure of the hetero boundaries, that is, armchair or zigzag. Li and Shenoy[154] have also verified the semiconducting property of the hybridized graphene patches embedded in boron nitride single-layer and the dependence of energy gaps upon the size of graphene patches. Jun et al.[155] have investigated the elastic properties of hybridized graphene and boron nitride mono-layer superlattices by density-functional theory calculations. They defined boundary stress of 2-D heterophase monolayers and computed the boundary stress of zigzag and armchair boundaries between graphene and boron nitride stripes. They showed that armchair boundary stress is correlated with energy gaps through the threefold oscillating behavior. On the other hand, zigzag boundary stresses are negligibly small regardless of stripe width, which indicates

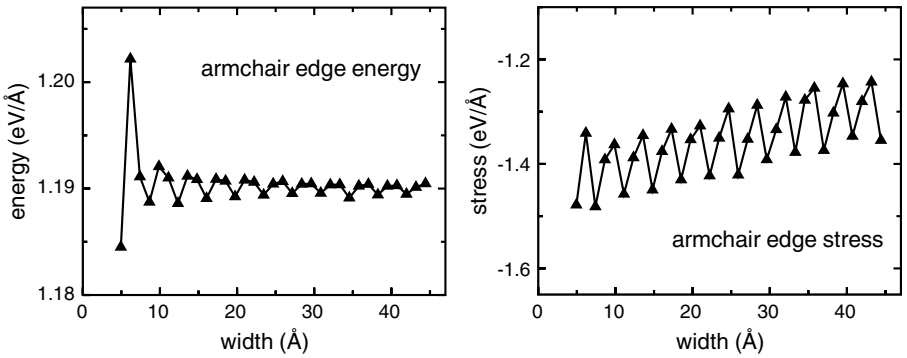

Fig. 4 Threefold oscillatory behavior of edge energy and edge stress of armchair nanoribbons with respect to ribbon width.[149]

the elastic stability of zigzag boundary. In addition, the zigzag boundary stress is even smaller than the edge stresses of hydrogen-passivated individual graphene and boron nitride nanoribbons. It again means that zigzag boundaries are very stable and cause no intrinsic deformation.

4.2 *Strain-Induced Modification of the Electronic Properties of Graphene Nanoribbons*

The perfect graphene sheet, without edge defect, is a zero-gap semiconductor with the Dirac points at the six corners of 2-D hexagonal Brillouin zone.[17] However, the presence of edges induces changes in the electronic property of perfect graphene sheet. As mentioned above, hydrogen-terminated armchair graphene nanoribbons are semiconducting with direct energy gaps whose magnitudes vary with respect to ribbon width, following the threefold oscillation. In contrast, H-passivated zigzag graphene nanoribbons are metallic with the edge state due to the edge defect.[146] Furthermore, Son et al.[150] discovered that zigzag graphene nanoribbons become half-metallic under external electric field.

Lee and Choi[156] have recently performed comprehensive spin-polarized electronic structure calculations of graphene nanoribbons by considering a variety of edge terminations. The spin-resolved band structures of a H-terminated zigzag nanoribbon are shown in Fig. 5 for three kinds of spin configuration (PM: without spin polarization, FA: ferromagnetic spin ordering at each edge and antiparallel spin orientation between both the edges, and FF: ferromagnetic spin ordering between both the edges. Local density approximation and spin-polarized numerical basis were used for the calculations of band structures in Fig. 5. Spin up and down bands are drawn by red solid and dashed blue lines, respectively. In the spin-unpolarized PM band structure, the degenerated highest occupied and lowest unoccupied bands are flat in the vicinity of the X point, indicating the edge state. When considering spin polarization, the total energy, calculated in the context of local density approximation density-functional theory, tends to be lowered by the breaking of spin degeneracy or the opening of energy gap. As shown in the middle panel of Fig. 5, the FA band structure yields a small energy gap but still keeps the degeneracy between both spins. In contrast, no gap opening is observed in the FF band structure (right panel of Fig. 5) because either one of spin up or down bands tends to be occupied to cause the system to become ferromagnetic, and as a result, each spin band crosses the Fermi level near $k = 2\pi/3$.[156]

Mechanical strain is often applied as a means to change the physical properties of carbon nanostructures. Several experimental studies have recently reported on the strain-induced modification of electronic properties of graphene. Strain can be applied to graphene specimens by bending substrates or directly pushing them using the tip of an atomic force microscope. Motivated by recent works pointing to a remarkable stability of graphene with large strains, Choi et al.[157] have carried out first-principles calculations and theoretical analysis to explore the electronic structures of strained graphene sheet. They showed that strained graphene does not develop an energy gap with the semimetallic nature being preserved up to a 30% applied uniaxial strain. It was also shown that the group velocities under uniaxial strain exhibit a strong anisotropy and the work function of strained graphene increases substantially as strain

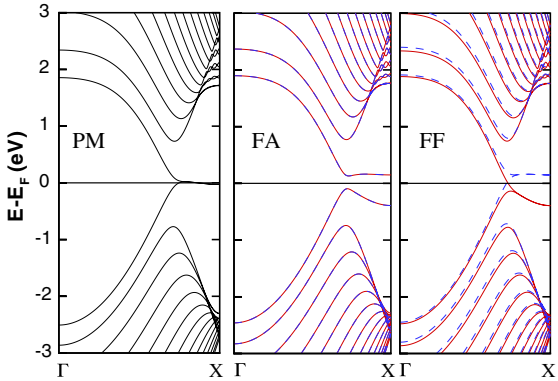

Fig. 5 Electronic band structures of zigzag graphene nanoribbons.[156]

increases.[157] On the other hand, results of first-principles calculations by Ni et al.[158] suggested that the energy gap opening of about 300 meV can be achieved by applying 1% uniaxial strain on graphene sheet. Gui et al.[159] have also reported that the band gap of strained graphene sheet can be tuned not only by the strain but also by the direction of the strain.

Electronic properties of graphene nanoribbons are sensitive to mechanical strain depending upon the edge type. Sun et al.[160] have calculated the electronic structures of deformed graphene nanoribbons using *ab initio* and tight-binding methods. They found that the energy gaps of armchair ribbons change with zigzag shape as a function of the applied uniaxial strain and the tunable window of the energy gap becomes narrower when the width of armchair nanoribbons increases. Interestingly, the closing of the bandgap and metallic state are not really achieved. This is due to an electron-phonon interaction Peierls-like effect.[161] In contrast, the electronic property of zigzag graphene nanoribbons was found to be insensitive to uniaxial strain. Sun et al.[160] have further performed spin-polarized calculations of the deformed zigzag ribbons. They observed that the states of opposite spin orientation are degenerated in all bands regardless of the strain condition and the band gap changes between 0.29 and 0.35 eV for the zigzag ribbons with −5.0% and +5.0% strain. Therefore, the deformed zigzag graphene nanoribbons are semiconductor and that the energy gaps are tuned less significantly than armchair ribbons by external strain.

Liu et al.[162] have investigated the uniaxial strain effect on the band structure of zigzag graphene nanoribbons within the mean-field Hubbard model. They found that the uniaxial strain influences electron distribution along edges and changes the intrinsic gap around the Fermi energy. When the compressive strain along the armchair direction and the tensile strain along the zigzag direction are applied above 13%, the conduction band and the valence band are split and gaps appear in addition to the modification of the intrinsic energy gap. because uniaxial strain breaks the lattice symmetry and causes two different hopping energies. Strain thus impacts the ratio of the two different hopping energies, which determines the intrinsic gap and the strain-induced gap. Using first-principles calculations, Jun et al.[163] has recently studied strain effects on the electronic and spin proeperties of 2-D hybrid superlattices that consist of alternating graphene and boron nitride mono-layer stripes. Fig. 6 shows the energy gap landscape with respect to the applied strains and stripe widths, when tensile strains are applied perpendicular to the boundary direction. Similar to graphene nanoribbons, energy gaps significantly vary by not only stripe width but applied strain.

The electronic behavior of H-terminated twisted graphene nanoribbons has been studied by Gunlycke et al.[164] and by Zhang and Dumitrică[121] who proposed that the band gap is determined by an effective tensional strain, Fig. 7. The effective strain, defined as the average tensile strain around the circumference, depends quadratically on the applied twist. Microscopic simulations uncovered an atypical coupling of the twist with axial shrinking that critically impacts the bandgap variations and points to significant electromechanical differences between free-standing

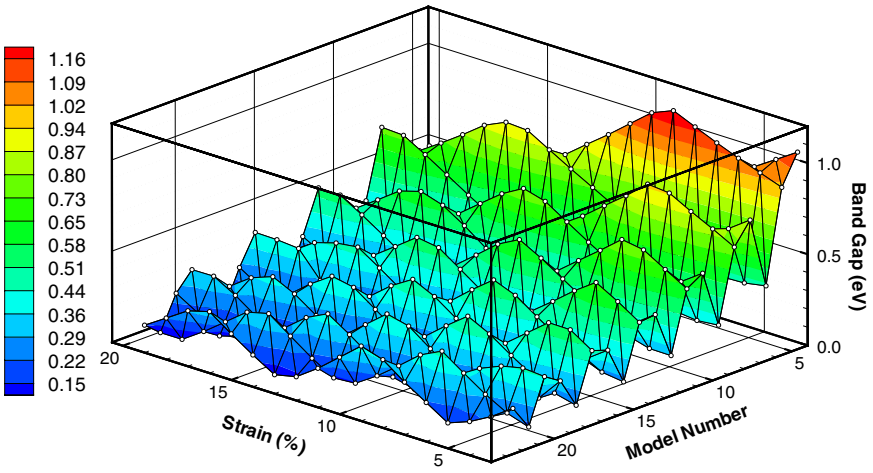

Fig. 6 Strain-dependent variations of the energy gap for the armchair hybrid graphene-BN monolayer superlattices.[163] Model number implies the number of armchair dimer lines in each stripe of a superlattice (i.e., the width of stripes).

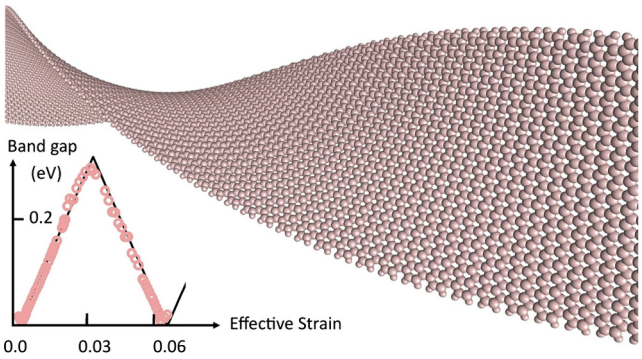

Fig. 7 A twisted 41-GNR. The insert shows its band gap modulation versus effective tensile strain, which appears similar to the one of a nanoribbon in tension, see Fig. 6. (Adapted from Ref. 121).

and suspended graphene nanoribbons. Due to this inverse-Poynting effect,[165] suspended graphene nanoribbons appear best suited for band gap tunability under twist. The concept of an effective strain might be largely useful for understanding the electromechanical behavior of other non-ideal graphene forms, including helical rippled carbon nanotubes.[166]

Ab initio studies of the optical spectra of graphene nanoribbons have been carried out by Prezzi et al.[167] and Yang et al.[168] Because of the reduced dimensionality of these structures, the optical response is dominated by prominent excitonic peaks. The binding energy of excitons in armchair nanoribbons with widths around 1.2 nm was found to be $0.8 - 1.4$ eV.

5 Summary

Fabrication methodologies and the combination of ideal properties of graphene present large interest for different areas of engineering. We reviewed progress in substrate-supported graphene growth, and in the fundamental understanding of mechanical, electronic, and optical properties, with an emphasis on graphene nanoribbons.

Acknowledgments

T.D. acknowledges support from NSF Grant No. DMR-1006706, NSF CAREER Grant No. CMMI-0747684, and AFOSR Grant No. FA9550-09-1-0339. S.K. thanks the UCLA COR Faculty Grants Program for the support. S. J. was supported by the Converging Research Center Program through the Ministry of Education, Science and Technology of Korea (2011K000622) and by NSF through Grant No. CMMI-0856250.

References

1. K. S. Novoselov et al, "Electric field effect in atomically thin carbon films," *Science* **306**, 666–669 (2004). http://dx.doi.org/10.1126/science.1102896.
2. K. I. Bolotin et al., "Ultrahigh electron mobility in suspended graphene," *Solid State Communications* **146**, 351–355 (2008). http://dx.doi.org/10.1016/j.ssc.2008.02.024.
3. Y. Shi et al., "Photoelectrical response in single-layer graphene transistor," *Small* **5**, 2005 (2009). http://dx.doi.org/10.1002/smll.v5:17.
4. A. K. Geim and K. S. Novoselov, "The rise of graphene," *Nat. Mat.* **6**, 183–191 (2007). http://dx.doi.org/10.1038/nmat1849.
5. C. Lee et al., "Measurement of the elastic properties and intrinsic strength of monolayer graphene," *Science* **321**, 385–388 (2008). http://dx.doi.org/10.1126/science.1157996
6. S. Ghosh et al., "Dimensional crossover of thermal transport in few-layer graphene," *Nat. Mater.* **9**, 555–558 (2010). http://dx.doi.org/10.1038/nmat2753.
7. A. K. Geim, "Graphene: Status and perspectives," *Science* **324**, 1530–1534 (2009). http://dx.doi.org/10.1126/science.1158877.

8. N. Mohanty and V. Berry, "Graphene-based single-bacterium resolution biodevice and DNA transistor: Interfacing graphene derivatives with nanoscale and microscale biocomponents," *Nano Lett.* **8**, 4469–4476 (2008). http://dx.doi.org/10.1021/nl802412n.
9. F. Bonaccorso et al., "Graphene photonics and optoelectronics," *Nat. Photon.* **4**, 611–622 (2010). http://dx.doi.org/10.1038/nphoton.2010.186.
10. T. Mueller, F. Xia, and P. Avouris, "Graphene photodetectors for high-speed optical communications," *Nat. Photon.* **4**, 297–301 (2010). http://dx.doi.org/10.1038/nphoton.2010.40.
11. Z. Sun et al., "Graphene mode-locked ultrafast laser," *ACS Nano* **4**, 803–810 (2010). http://dx.doi.org/10.1021/nn901703e
12. H. J. Mamin and D. Rugar, "Sub-attonewton force detection at millikelvin temperatures," *Appl. Phys. Lett.* **79**, 3358–3360 (2001). http://dx.doi.org/10.1063/1.1418256.
13. L. Gong et al., "Interfacial stress transfer in a graphene monolayer manocomposite," *Adv. Mater.* **22**, 2694–2697 (2010). http://dx.doi.org/10.1002/adma.200904264
14. R. J. Young et al., "Strain mapping in a graphene monolayer nanocomposite," *ACS Nano* **5**(4), 3079–3084 (2011). http://dx.doi.org/10.1021/nn2002079.
15. J. S. Bunch et al., "Electromechanical resonators from graphene sheets," *Science* **315**, 490–493 (2007). http://dx.doi.org/10.1126/science.1136836.
16. J. S. Bunch et al., "Impermeable atomic membranes from graphene sheets," *Nano Lett.* **8**(8), 2458–2462 (2008). http://dx.doi.org/10.1021/nl801457b.
17. H. Castro Neto et al., "The electronic properties of graphene," *Rev. Mod. Phys.* **81**, 109–162 (2009). http://dx.doi.org/10.1103/RevModPhys.81.109.
18. Z. H. Ni et al., "Uniaxial strain on graphene: Raman spectroscopy study and band-gap opening," *ACS Nano* **2**, 2301–2305 (2008). http://dx.doi.org/10.1021/nn800459e
19. B. Partoens and F. M. Peeters, "From graphene to graphite: Electronic structure around the k point," *Phys. Rev. B* **74**, 075404 (2006). http://dx.doi.org/10.1103/PhysRevB.74.075404.
20. K. F. Maka et al., "The evolution of electronic structure in few-layer graphene revealed by optical spectroscopy," *Proc. Natl. Acad. Sci.* **107**, 14999–15004 (2010). http://dx.doi.org/10.1073/pnas.1004595107
21. L. Liao et al., "High-speed graphene transistors with a self-aligned nanowire gate," *Nature* **467**, 305–308 (2010). http://dx.doi.org/10.1038/nature09405
22. Y.-M. Lin et al., "Wafer-scale graphene integrated circuit," *Science* **332**, 1294–1297 (2011). http://dx.doi.org/10.1126/science.1204428
23. T. Gokus et al., "Making graphene luminescent by oxygen plasma treatment," *ACS Nano* **3**, 3963–3968 (2009). http://dx.doi.org/10.1021/nn9012753.
24. R. J. Stohr et al., "Fluorescence of laser-created electron-hole plasma in graphene," *Phys. Rev. B* **82**, 121408(R) (2001). http://dx.doi.org/10.1103/PhysRevB.82.121408
25. D. R. Dreyer et al., "The chemistry of graphene oxide," *Chem. Soc. Rev.* **39**, 228–240 (2009). http://dx.doi.org/10.1039/b917103g.
26. Y. W. Zhu et al., "Graphene and graphene oxide: Synthesis, properties, and applications," *Adv. Mater.* **22**, 3906–3924 (2010). http://dx.doi.org/10.1002/adma.201001068
27. G. Eda and M. Chhowalla, "Chemically derived graphene oxide: Towards large-area thin-film electronics and optoelectronics," *Adv. Mater.* **22**, 2392–2415 (2010). http://dx.doi.org/10.1002/adma.200903689
28. O. C. Compton and S. T. Nguyen, "Graphene oxide, highly reduced graphene oxide, and graphene: Versatile building blocks for carbon-based materials," *Small* **6**, 711–723 (2010), http://dx.doi.org/10.1002/smll.v6:6.
29. W. C. Ren et al., "Preparation of graphene by chemical vapor deposition," *New Carbon Mater.* **26**, 71–80 (2011).
30. K. S. Novoselov et al., "Two-dimensional atomic crystals," *Proc. Natl. Acad. Sci. USA* **102**, 10451 (2005). http://dx.doi.org/10.1073/pnas.0502848102.
31. K. I. Bolotin et al., "Ultrahigh electron mobility in suspended graphene," *Solid State Commun.* **146**, 351–355 (2008). http://dx.doi.org/10.1016/j.ssc.2008.02.024.
32. M. Y. Han et al., "Energy band-gap engineering of graphene nanoribbons," *Phys. Rev. Lett.* **98**, 206805 (2007). http://dx.doi.org/10.1103/PhysRevLett.98.206805
33. K. Nakada et al., "Edge state in graphene ribbons: Nanometer size effect and edge shape dependence," *Phys. Rev. B* **54**, 17954 (1996). http://dx.doi.org/10.1103/PhysRevB.54.17954.

34. Y.-W. Son, M. L. Cohen, and S. G. Louie, "Half-metallic graphene nanoribbons," *Nature* **444**, 347 (2006). http://dx.doi.org/10.1038/nature05180.
35. X. Li et al., "Chemically derived, ultrasmooth graphene nanoribbon semiconductors," *Science* **319**, 1229 (2008).
36. J. W. Bai et al., "Graphene nanomesh," *Nat. Nanotechnol.* **5**(3), 190–194 (2010). http://dx.doi.org/10.1038/nnano.2010.8.
37. L. P. Biro and P. Lambin, "Nanopatterning of graphene with crystallographic orientation control," *Carbon* **48**, 2677–2689 (2010). http://dx.doi.org/10.1016/j.carbon.2010.04.013.
38. J. W. Bai and Y. Huang, "Fabrication and electrical properties of graphene nanoribbons," *Mater. Sci. Eng. R-Rep.* **70**, 341–353 (2010). http://dx.doi.org/10.1016/j.mser.2010.06.019.
39. X. L. Li et al., "Chemically derived, ultrasmooth graphene nanoribbon semiconductors," *Science* **319**, 1229–1232 (2008). http://dx.doi.org/10.1126/science.1150878
40. S. Park and R. S. Ruoff, "Chemical methods for the production of graphenes," *Nat. Nanotechnol.* **4**, 217–224 (2009). http://dx.doi.org/10.1038/nnano.2009.58
41. X. Cui et al., "Liquid-phase exfoliation, functionalization and applications of graphene," *Nanoscale* **3**, 2118–2126 (2011). http://dx.doi.org/10.1039/C1NR10127G
42. L. M. Viculis, J. J. Mack, and R. B. Kaner, "A chemical route to carbon nanoscrolls," *Science* **299**, 1361 (2003). http://dx.doi.org/10.1126/science.1078842.
43. A. Dimiev et al., "Layer-by-layer removal of graphene for device patterning," *Science* **331**, 1168–1172 (2011). http://dx.doi.org/10.1126/science.1199183.
44. L. Kubler et al., "Bidimensional intercalation of Ge between SiC(0001) and a heteroepitaxial graphite top layer," *Phys. Rev. B* **72**, 115319 (2005). http://dx.doi.org/10.1103/PhysRevB.72.115319.
45. A. J. Van Bommel, J. E. Crombeen, and A. Van Tooren, "LEED and Auger electron observations of the SiC(0001) surface," *Surf. Sci.* **48**, 463 (1975). http://dx.doi.org/10.1016/0039-6028(75)90419-7.
46. I. Forbeaux et al. and J.-M. Debever, "Solid-state graphitization mechanisms of silicon carbide 6HSiC polar faces," *Appl. Surf. Sci.* **162**, 406 (2000). http://dx.doi.org/10.1016/S0169-4332(00)00224-5.
47. A. Charrier et al., "Solid-state decomposition of silicon carbide for growing ultra-thin heteroepitaxial graphite films," *J. Appl. Phys.* **92**, 2479 (2002). http://dx.doi.org/10.1063/1.1498962.
48. I. Forbeaux, J.-M. Themlin, and J.-M. Debever, "Heteroepitaxial graphite on 6H-SiC(0001): Interface formation through conduction-band electronic structure," *Phys. Rev. B* **58**, 16396 (1998). http://dx.doi.org/10.1103/PhysRevB.58.16396.
49. I. Forbeaux, J.-M. Themlin, and J.-M. Debever, "High-temperature graphitization of the 6H-SiC (0001) face," *Surf. Sci.* **442**, 9 (1999). http://dx.doi.org/10.1016/S0039-6028(99)00891-2.
50. M. Sprinkle et al., "Scalable templated growth of graphene nanoribbons on SiC," *Nat. Nanotechnol.* **5**, 727 (2010). http://dx.doi.org/10.1038/nnano.2010.192.
51. J. S. Moon et al., "Top-gated epitaxial graphene FETs on Si-face SiC wafers with a peak transconductance of 600 ms/mm," *IEEE Electron Device Lett.* **31**, 260 (2010). http://dx.doi.org/10.1109/LED.2010.2040132
52. C. Dimitrakopoulos et al., "Wafer-scale epitaxial graphene growth on the Si-face of hexagonal SiC (0001) for high frequency transistors," *J. Vac. Sci. Technol. B* **28**, 985 (2010). http://dx.doi.org/10.1116/1.3480961.
53. J. S. Moon et al., "Self-aligned graphene-on-SiC and graphene-on-Si MOSFETs on 75 mm wafers," DRC , pp 209, (2010). http://dx.doi.org/10.1109/DRC.2010.5551910
54. C. Riedl et al., "Quasi-free-standing epitaxial graphene on sic obtained by hydrogen intercalation," *Phys. Rev. Lett.* **103**, 246804 (2009). http://dx.doi.org/10.1103/PhysRevLett.103.246804.
55. S. Oida et al., "Decoupling graphene from SiC(0001) via oxidation," *Phys. Rev. B* **82**, 041411 (2010). http://dx.doi.org/10.1103/PhysRevB.82.041411.
56. L. Luxmi et al., "Comparison of graphene formation on C-face and Si-face SiC 0001 surfaces," *Phys. Rev. B* **82**, 235406 (2010). http://dx.doi.org/10.1103/PhysRevB.82.235406.

57. J. Hass, W. A. de Heer, and E. H. Conrad, "The growth and morphology of epitaxial multilayer graphene," *J. Phys.: Condens. Matter.* **20**, 323202 (2008). http://dx.doi.org/10.1088/0953-8984/20/32/323202.
58. T. Seyller et al., "Epitaxial graphene: a new material," *Phys. Status Solidi B-Basic Solid State Phys.* **245**, 1436–1446 (2008), http://dx.doi.org/10.1002/pssb.v245:7.
59. J. B. Hannon and R. M. Tromp, "Pit formation during graphene synthesis on SiC(0001): In situ electron microscopy," *Phys. Rev. B* **77**, 241404 (2008). http://dx.doi.org/10.1103/PhysRevB.77.241404.
60. T. Ohta et al., "Morphology of graphene thin film growth on SiC(0001)," *New J. Phys.* **10**, 023034 (2008). http://dx.doi.org/10.1088/1367-2630/10/2/023034. .
61. J. B. Hannon et al., "Spontaneous formation and growth of a new polytype on SiC(0001)," *Phys. Rev. Lett.* **103**, 256101 (2009). http://dx.doi.org/10.1103/PhysRevLett.103.256101.
62. H. Hibino et al., "Stacking domains of epitaxial few-layer graphene on SiC(0001)," *Phys. Rev. B* **80**, 085406 (2009). http://dx.doi.org/10.1103/PhysRevB.80.085406.
63. H. Hibino, H. Kageshima, and M. Nagase, "Epitaxial few-layer graphene: Towards single crystal growth," *J. Phys. D: Appl. Phys.* **43**, 374005 (2010). http://dx.doi.org/10.1088/0022-3727/43/37/374005.
64. S. Tanaka, K. Morita, and H. Hibino, "Anisotropic layer-by-layer growth of graphene on vicinal SiC(0001) surfaces," *Phys. Rev. B* **81**, 041406 (2010). http://dx.doi.org/10.1103/PhysRevB.81.041406
65. R. M. Tromp and J. B. Hannon, "Thermodynamics and kinetics of graphene growth on SiC(0001)," *Phys. Rev. Lett.* **102**, 106104 (2009). http://dx.doi.org/10.1103/PhysRevLett.102.106104.
66. W. J. Lu, J. J. Boeckl, and W. C. Mitchel, "A critical review of growth of low-dimensional carbon nanostructures on SiC (0001): impact of growth environment," *J. Phys. D: Appl. Phys.* **43**, 374004 (2010). http://dx.doi.org/10.1088/0022-3727/43/37/374004
67. Z. Sun et al., "Growth of graphene from solid carbon sources," *Nature* **468**, 549–552 (2010). http://dx.doi.org/10.1038/nature09579.
68. M. Z. M. Zheng et al., "Metal-catalyzed crystallization of amorphous carbon to graphene," *Appl. Phys. Lett.* **96**, 063110 (2010). http://dx.doi.org/10.1063/1.3318263
69. Y. Murata et al., "Moire superstructures of graphene on faceted nickel islands," *ACS Nano* **4**, 6509–6514 (2010). http://dx.doi.org/10.1021/nn102446y.
70. M. S. Xu et al., "Production of extended single-layer graphene," *ACS Nano* **5**, 1522–1528 (2011). http://dx.doi.org/10.1021/nn103428k
71. L. C. Isett and J. M. Blakely, "Segregation isosteres for carbon at (100) surface of nickel," *Surf. Sci.* **58**, 397–414 (1976). http://dx.doi.org/10.1016/0039-6028(76)90478-7.
72. M. Eizenberg and J. M. Blakely, "Carbon monolayer phase condensation on NI(111)," *Surf. Sci.* **82**, 228–236 (1979). http://dx.doi.org/10.1016/0039-6028(79)90330-3.
73. J. C. Hamilton and J. M. Blakely, "Carbon segregation to single-crystal surfaces of Pt, Pd and Co," *Surf. Sci.* **91**, 199–217 (1980). http://dx.doi.org/10.1016/0039-6028(80)90080-1.
74. R. Rosei et al., "Structure of graphitic carbon on Ni(111): A surface extended-energy-loss fine-structure study," *Phys. Rev. B* **28**, 1161 (1983). http://dx.doi.org/10.1103/PhysRevB.28.1161.
75. N. A. Kholin, E. V. Rut'kov, and A. Y. Tontegode, "The nature of the adsorption bond between graphite islands and iridium surface," *Surf. Sci.* **139**, 155 (1984). http://dx.doi.org/10.1016/0039-6028(84)90014-1.
76. H. Zi-pu et al., "LEED theory for incommensurate overlayers: Application to graphite on Pt (111)," *Surf. Sci.* **180**, 433 (1987). http://dx.doi.org/10.1016/0039-6028(87)90219-6.
77. T. A. Land et al., "STM investigation of single layer graphite structures produced on Pt(111) by hydrocarbon decomposition," *Surf. Sci.* **264**, 261 (1992). http://dx.doi.org/10.1016/0039-6028(92)90183-7.
78. T. Aizawa et al., "Anomalous bond of monolayer graphite on transition-metal carbide surfaces," *Phys. Rev. Lett.* **64**, 768 (1990). http://dx.doi.org/10.1103/PhysRevLett.64.768.
79. H. Itoh et al., "Scanning tunneling microscopy of monolayer graphite epitaxially grown on a TiC(111) surface," *Surf. Sci.* **254**, 437 (1991). http://dx.doi.org/10.1016/0039-6028(91)90620-8.

80. P. M. Stefan et al., "Photoemission study of WC(0001)," *Phys. Rev. B* **29**, 5423 (1984). http://dx.doi.org/10.1103/PhysRevB.29.5423.
81. C. Oshima et al., "Carbon layer on lanthanum hexaboride (100) surface," *Jpn. J. Appl. Phys.* **16**, 965 (1977). http://dx.doi.org/10.1143/JJAP.16.965.
82. C. Oshima et al., "A hetero-epitaxial-double-atomic-layer system of monolayer graphene/monolayer h-BN on Ni(111)," *Sol. State Commun.* **116**, 37 (2000). http://dx.doi.org/10.1016/S0038-1098(00)00268-4.
83. C. Oshima and A. Nagashima, "Ultra-thin epitaxial films of graphite and hexagonal boron nitride on solid surfaces," *J. Phys.: Condens. Matter.* **9**, 1 (1997). http://dx.doi.org/10.1088/0953-8984/9/1/004, and references therein.
84. T. Oznuluer et al., "Synthesis of graphene on gold," *Appl. Phys. Lett.* **98**, 183101 (2011). http://dx.doi.org/10.1063/1.3584006.
85. J. Coraux et al., "Growth of graphene on Ir(111)," *J. New Phys.* **11**, 023006 (2009). http://dx.doi.org/10.1088/1367-2630/11/3/039801.
86. S. Marchini, S. Gnther, and J. Wintterlin, "Scanning tunneling microscopy of graphene on Ru (0001)," *Phys. Rev. B* **76**, 075429 (2007). http://dx.doi.org/10.1103/PhysRevB.76.075429.
87. A. L. Vazquez de Parga et al., "Periodically rippled graphene: Growth and spatially resolved electronic structure," *Phys. Rev. Lett.* **100**, 056807 (2008). http://dx.doi.org/10.1103/PhysRevLett.100.056807.
88. P. W. Sutter, J.-I. Flege, and E. A. Sutter, "Epitaxial graphene on ruthenium," *Nat. Mater.* **7**, 406 (2008). http://dx.doi.org/10.1038/nmat2166.
89. Y. Pan et al., "Highly ordered single crystalline graphene grown on Ru(0001) surface," arxiv0709.2858.
90. S. Y. Kwon et al., "Growth of semiconducting graphene on palladium," *Nano Lett.* **9**, 3985–3990 (2009). http://dx.doi.org/10.1021/nl902140j.
91. Q. Yu et al., "Graphene synthesis by surface segregation on Ni and Cu," arxiv0804.1778.
92. S. J. Chae et al., "Synthesis of large-area graphene layers on poly-nickel substrate by chemical vapor deposition: Wrinkle formation," *Adv. Mater.* **21**, 2328 (2009). http://dx.doi.org/10.1002/adma.v21:22.
93. G. Nandamuri, S. Roumimov, and R. Solanki, "Chemical vapor deposition of graphene films," *Nanotechnology* **21**, 145604 (2010). http://dx.doi.org/10.1088/0957-4484/21/14/145604.
94. P. Sutter, J. T. Sadowski, and E. Sutter, "Graphene on Pt(111): Growth and substrate interaction," *Phys. Rev. B* **80**, 245411 (2009). http://dx.doi.org/10.1103/PhysRevB.80.245411.
95. G. Imamura and K. Saiki, "Synthesis of nitrogen-doped graphene on Pt(111) by chemical vapor deposition," *J. Phys. Chem. C* **115**, 10000–10005 (2011). http://dx.doi.org/10.1021/jp202128f.
96. J. H. Gao et al., "Unique synthesis of few-layer graphene films on carbon-doped Pt(83)Rh (17) surfaces," *ACS Nano* **4**, 1026–1032 (2010). http://dx.doi.org/10.1021/nn901255u
97. Y. Murata et al., "Orientation-dependent work function of graphene on Pd(111)," *Appl. Phys. Lett.* **97**, 143114 (2010). http://dx.doi.org/10.1063/1.3495784.
98. E. Loginova et al., "Evidence for graphene growth by C cluster attachment," *New J. Phys.* **10**, 093026 (2008), http://dx.doi.org/10.1088/1367-2630/10/9/093026.
99. E. Loginova et al., "Factors influencing graphene growth on metal surfaces," *J. New Phys.* **11**, 063046 (2009). http://dx.doi.org/10.1088/1367-2630/11/6/063046.
100. E. Loginova et al., "Defects of graphene on Ir(111): Rotational domains and ridges," *Phys. Rev. B* **80**, 085430 (2009). http://dx.doi.org/10.1103/PhysRevB.80.085430.
101. K. F. McCarty et al., "Kinetics and thermodynamics of carbon segregation and graphene growth on Ru(0001)," *Carbon* **47**, 1806–1813 (2009). http://dx.doi.org/10.1016/j.carbon.2009.03.004.
102. E. Starodub et al., "Graphene growth by metal etching on Ru(0001)," *Phys. Rev. B* **80**, 235422 (2009). http://dx.doi.org/10.1103/PhysRevB.80.235422.
103. E. Starodub, N. C. Bartelt, and K. F. McCarty, "Oxidation of graphene on metals," *J. Phys. Chem. C* **114**, 5134–5140 (2010). http://dx.doi.org/10.1021/jp912139e.
104. J. M. Wofford et al., "Graphene islands on Cu foils: The interplay between shape, orientation, and effects," *Nano Lett.* **10**, 4890–4896 (2010). http://dx.doi.org/10.1021/nl102788f.

105. S. Nie et al., "Growth from below: Graphene bilayers on Ir(111)," *ACS Nano* **5**, 2298–2306 (2011). http://dx.doi.org/10.1021/nn103582g.
106. K. S. Kim et al., "Large-scale pattern growth of graphene films for stretchable transparent electrodes," *Nature* **457**, 706–710 (2009). http://dx.doi.org/10.1038/nature07719
107. X. S. Li et al., "Large-area synthesis of high-quality and uniform graphene films on copper foils," *Science* **324**, 1312–1314 (2009). http://dx.doi.org/10.1126/science.1171245
108. C. M. C. Mattevi, H. Kim, and M. Chhowalla, "A review of chemical vapour deposition of graphene on copper," *J. Mater. Chem.* **21**, 3324–3334 (2011). http://dx.doi.org/10.1039/c0jm02126a.
109. S. S. Datta et al., "Crystallographic etching of few-layer graphene," *Nano Lett.* **8**, 19121915 (2008). http://dx.doi.org/10.1021/nl080583r.
110. X. Li et al., "Chemically derived, ultrasmooth graphene nanoribbon semiconductors," *Science* **319**, 12291232 (2008).
111. L. Y. Jiao et al., "Narrow graphene nanoribbons from carbon nanotubes," *Nature* **458**, 877–880 (2009). http://dx.doi.org/10.1038/nature07919.
112. L. Jiao et al., "Facile synthesis of high-quality graphene nanoribbons," *Nat. Nanotechnol.* **5**, 321–325 (2010). http://dx.doi.org/10.1038/nnano.2010.54.
113. A. Chuvilin et al., "Self-assembly of a sulphur-terminated graphene nanoribbon within a single-walled carbon nanotube," *Nat. Mater.* **10**, 687–692 (2011). http://dx.doi.org/10.1038/nmat3082.
114. Z. Xu and M. J. Buehler, "Geometry controls conformation of graphene sheets: Membranes, ribbons, and scrolls," *ACS Nano* **4**, 3869 (2010). http://dx.doi.org/10.1021/nn100575k
115. H. C. Schniepp et al., "Bending properties of single functionalized graphene sheets probed by atomic force microscopy," *ACS Nano* **2**, 2577–2584 (2008). http://dx.doi.org/10.1021/nn800457s.
116. J. Zhang et al., "Free folding of suspended graphene sheets by random mechanical stimulation," *Phys. Rev. Lett.* **104**, 166805 (2010). http://dx.doi.org/10.1103/PhysRevLett.104.166805
117. A. L. Vazquez de Parga et al., "Periodically rippled graphene: Growth and spatially resolved electronic structure multiply folded graphene," *Phys. Rev. Lett.* **100**, 056807 (2008). http://dx.doi.org/10.1103/PhysRevLett.100.056807.
118. K. Kim et al., "Multiply folded graphene," *Phys. Rev. B* **83**, 245433 (2011)
119. M. M. Fogler, A. H. Castro Neto, and F. Guinea, "Effect of external conditions on the structure of scrolled graphene edges," *Phys. Rev. B* **81**, 161408(R) (2010). http://dx.doi.org/10.1103/PhysRevB.81.161408.
120. V. B. Shenoy et al., "Edge-stress-induced warping of graphene sheets and nanoribbons," *Phys. Rev. Lett.* **101**, 245501 (2008). http://dx.doi.org/10.1103/PhysRevLett.101.245501.
121. D.-B. Zhang and T. Dumitrică, "Effective tensional-strain driven bandgap modulations in helical graphene nanoribbons," *Small* **7**, 1023 (2011). http://dx.doi.org/10.1002/smll.201001890
122. M. Poot and H. S. J. van der Zant, "Nanomechanical properties of few-layer graphene membranes," *Appl. Phys. Lett.* **92**, 063111 (2008). http://dx.doi.org/10.1063/1.2857472.
123. D. Garcia-Sanchez et al., "Imaging mechanical vibrations in suspended graphene sheets," *Nano Lett.* **8**, 1399–1403 (2008). http://dx.doi.org/10.1021/nl080201h. .
124. D. C. Wei et al., "Scalable synthesis of few-layer graphene ribbons with controlled morphologies by a template method and their applications in nanoelectromechanical switches," *Am. J. Chem. Soc.* **131**, 11147–11154 (2009). http://dx.doi.org/10.1021/ja903092k
125. M. Dragoman et al., "Microwave switches based on graphene," *J. Appl. Phys.* **105**, 054309 (2009). http://dx.doi.org/10.1063/1.3080130
126. C. Y. Chen et al., "Performance of monolayer graphene nanomechanical resonators with electric readout," *Nat. Nanotechnol.* **4**, 861–867 (2009). http://dx.doi.org/10.1038/nnano.2009.267.
127. O. A. Shenderova, V. V. Zhirnov, and D. W. Brenner, "Carbon nanostructures," *Crit. Rev. Solid State Mater. Sci.* **27**, 227–356 (2002). http://dx.doi.org/10.1080/10408430208500497.

128. O. L. Blackslee et al., "Elastic constants of compression-annealed pyrolytic graphite," *J. Appl. Phys.* **41**, 3373–3382 (1970). http://dx.doi.org/10.1063/1.1659428
129. J. Atalaya, A. Isacsson, and J. M. Kinaret, "Continuum elastic modeling of graphene resonators," *Nano Lett.* **8**, 4196–4200 (2008). http://dx.doi.org/10.1021/nl801733d.
130. L. F. Wang et al., "Size dependence of the thin-shell model for carbon nanotubes," *Phys. Rev. Lett.* **95**, 105501 (2005). http://dx.doi.org/10.1103/PhysRevLett.95.105501
131. M. Arroyo and T. Belytschko, "Finite crystal elasticity of carbon nanotubes based on the exponential Cauchy-Born rule," *Phys. Rev. B* **69**, 115415 (2004). http://dx.doi.org/10.1103/PhysRevB.69.115415.
132. Y. Huang, J. Wu, and K. C. Hwang, "Thickness of graphene and single-wall carbon nanotubes," *Phys. Rev. B* **74**(24), 245413 (2006). http://dx.doi.org/10.1103/PhysRevB.74.245413.
133. M. Huang et al., "Electronic mechanical coupling in graphene from in situ nanoindentation experiments and multiscale atomistic simulations," *Nano Lett.* **1**(3), 1241–1246 (2011). http://dx.doi.org/10.1021/nl104227t
134. J. C. Meyer et al., "The structure of suspended graphene sheets," *Nature* **446**, 60–63 (2007). http://dx.doi.org/10.1038/nature05545
135. G. Tsoukleri et al., "Subjecting a graphene monolayer to tension and compression," *Small* **5**(21), 2397–2402 (2008). http://dx.doi.org/10.1002/smll.200900802
136. O. Frank et al., "Compression behavior of single-layer graphenes," *ACS Nano* **4**(6), 3131–3138 (2010). http://dx.doi.org/10.1021/nn100454w.
137. D.-B. Zhang, E. Akatyeva, and T. Dumitrică, "Bending ultrathin graphene at the margins of continuum mechanics," *Phys. Rev. Lett.* **106**, 255503 (2011). http://dx.doi.org/10.1103/PhysRevLett.106.255503
138. W. A. Harrison, *Elementary Electronic Structure* (World Scientific, 1999).
139. R. C. Haddon, "Chemistry of the fullerenes: The manifestation of strain in a class of continuous aromatic molecules," *Science* **261**, 1545–1550 (1993). http://dx.doi.org/10.1126/science.261.5128.1545.
140. R. C. Haddon, "Hybridization and the orientation and alignment of π-orbitals in nonplanar conjugated organic molecules: π-orbital axis vector analysis (POAV2)," *Am. J. Chem. Soc.* **108**, 2837–2842 (1986). http://dx.doi.org/10.1021/ja00271a009.
141. S. Niyogi et al., "Chemistry of single-walled carbon nanotubes," *Acc. Chem. Res.* **35**, 1105–1113 (2002). http://dx.doi.org/10.1021/ar010155r.
142. T. Dumitrică and R. D. James, "Objective molecular dynamics," *J. Mech. Phys. Solids* **55**, 2206–2236 (2007). http://dx.doi.org/10.1016/j.jmps.2007.03.001.
143. D.-B. Zhang, M. Hua, and T. Dumitrică, "Stability of polycrystalline and wurtzite Si nanowires via symmetry-adapted tight-binding objective molecular dynamics," *J. Chem. Phys.* **128**, 084104 (2008). http://dx.doi.org/10.1063/1.2837826
144. A. Carlson and T. Dumitrică, "Extended tight-binding potential for modeling intertube interactions in carbon nanotubes," *Nanotechnology* **18**, 065706 (2007). http://dx.doi.org/10.1088/0957-4484/18/6/065706
145. D. Porezag et al., "Construction of tight-binding-like potentials on the basis of density-functional theory: Application to carbon," *Phys. Rev. B* **51**, 12947–12957 (1995). http://dx.doi.org/10.1103/PhysRevB.51.12947.
146. K. Nakada et al., "Edge state in graphene ribbons: Nanometer size effect and edge shape dependence," *Phys. Rev. B* **54**, 17954–17961 (1996). http://dx.doi.org/10.1103/PhysRevB.54.17954.
147. R. C. Cammarata, "Surface and interface stress effects in thin films," *Prog. Surf. Sci.* **46**, 1–38 (1994). http://dx.doi.org/10.1016/0079-6816(94)90005-1.
148. S. Jun, "Density-functional study of edge stress in graphene," *Phys. Rev. B* **78**, 073405 (2008). http://dx.doi.org/10.1103/PhysRevB.78.073405
149. B. Huang et al., "Quantum manifestations of graphene edge stress and edge instability: A first-principles study," *Phys. Rev. Lett.* **102**, 166404 (2009). http://dx.doi.org/10.1103/PhysRevLett.102.166404
150. Y.-W. Son, M. L. Cohen, and S. G. Louie, "Half-metallic graphene nanoribbons," *Nature* **444**, 347–349 (2006). http://dx.doi.org/10.1038/nature05180.

151. L. Ci et al., "Atomic layers of hybridized boron nitride and graphene domains," *Nat. Mater.* **9**, 430–435 (2010). http://dx.doi.org/10.1038/nmat2711.
152. O. V. Yazyev and S. G. Louie, "Electronic transport in polycrystalline graphene," *Nat. Mater.* **9**, 806–809 (2010). http://dx.doi.org/10.1038/nmat2830.
153. J. M. Pruneda, "Origin of half-semimetallicity induced at interfaces of C-BN heterostructures," *Phys. Rev. B* **81**, 161409(R) (2010). http://dx.doi.org/10.1103/PhysRevB.81.161409.
154. J. Li and V. B. Shenoy, "Graphene quantum dots embedded in hexagonal boron nitride sheets," *Appl. Phys. Lett.* **98**, 013105 (2011). http://dx.doi.org/10.1063/1.3533804
155. S. Jun et al., "Elastic properties of edges in BN and SiC nanoribbons and of boundaries in C-BN superlattices: A density functional theory study," *Phys. Rev. B* **83**, 153407 (2011). http://dx.doi.org/10.1103/PhysRevB.83.153407.
156. G. Lee and K. Cho, "Electronic structures of zigzag graphene nanoribbons with edge hydrogenation and oxidation," *Phys. Rev. B* **79**, 165440 (2011). http://dx.doi.org/10.1103/PhysRevB.79.165440
157. S.-M. Choi, S.-H. Jhi, and Y.-W. Son, "Effects of strain on electronic properties of graphene," *Phys. Rev. B* **81**, 081407(R) (2010). http://dx.doi.org/10.1103/PhysRevB.81.081407
158. Z. H. Ni et al., "Uniaxial strain on graphene: Raman spectroscopy study and band-gap opening," *ACS Nano* **2**, 2301–2305 (2008).
159. G. Gui, J. Li, and J. Zhong, "Band structure engineering of graphene by strain: First-principles calculations," *Phys. Rev. B* **78**, 075435 (2008). http://dx.doi.org/10.1103/PhysRevB.78.075435.
160. L. Sun et al., "Strain effect on electronic structures of graphene nanoribbons: A first-principles study," *J. Chem. Phys.* **129**, 074704 (2008). http://dx.doi.org/10.1063/1.2958285
161. D.-B. Zhang and T. Dumitrică, "The role of Peierls-like distortions in the modification of electronic bandgaps of graphene nanoribbons under uniaxial strain," *J. Chem. Phys.* **134**, 196101 (2011). http://dx.doi.org/10.1063/1.3592526
162. F. Liu, X. Liu, and J. Kang, "Energy gap tuning in uniaxial strained zigzag graphene nanoribbons," *Appl. Phys. Lett.* **98**, 213502 (2011). http://dx.doi.org/10.1063/1.3593490
163. S. Jun et al., "Strain effects on the electronic and spin properties of 2d hybrid graphene and boron nitride monolayer superlattices," (in preparation).
164. D. Gunlycke et al., "Edges bring new dimension to graphene nanoribbons," *Nano Lett.* **10**, 3638 (2010). http://dx.doi.org/10.1021/nl102034c.
165. D.-B. Zhang and T. Dumitrică, "Role of the effective tensile strain in the electromechanical response of helical graphene nanoribbons with open and closed edges," *Phys. Rev.* **85**, 035445 (2012). http://dx.doi.org/10.1103/PhysRevB.85.035445
166. D.-B. Zhang and T. Dumitrică, "Effective shear strain in helical rippled carbon nanotubes: A unifying concept for understanding electromechanical response," *ACS Nano* **4**, 6966 (2010). http://dx.doi.org/10.1021/nn1019658
167. D. Prezzi et al., "Optical properties of graphene nanoribbons: The role of many-body effects," *Phys. Rev. B* **77**, 041404(R) (2008). http://dx.doi.org/10.1103/PhysRevB.77.041404
168. L. Yang, M. L. Cohen, and S. G. Louie, "Excitonic effects in the optical spectra of graphene nanoribbons," *Nano Lett.* **7**, 3112–3115 (2007). http://dx.doi.org/10.1021/nl0716404

Traian Dumitrică is an associate professor of mechanical engineering and a graduate faculty member in chemical engineering and materials science at the University of Minnesota, Twin Cities. His research focuses on understanding the mechanical properties of materials using advanced atomistic computational methods, and has involved problems arising in nanotechnology, mechanical engineering, and materials science. He has published over 40 refereed papers and several of his research projects have been featured in the press, including the New York Science Times. He is a recipient of the 2008 NSF CAREER award.

Suneel Kodambaka is an assistant professor of materials science engineering at the University of California Los Angeles. His research emphasizes the use of in situ TEM, LEEM, and high-temperature STM to quantitatively describe the kinetics of nucleation, growth, and thermal stability of nanocrystals, nanowires, graphene, and thin films. He received the 2010 Alumni Achievement award from the College of Engineering, SIUC; 2009 Paul Holloway Young Investigator Award from the AVS; 2008 Best Paper award from the IBM Materials Research Community; 2003 Ross J. Martin award from College of Engineering at UIUC and 2001 MRS Spring Gold medal for outstanding graduate research. Suneel can be reached at kodambaka@ucla.edu.

Sukky Jun received his PhD in mechanical engineering from Northwestern University. He is currently an assistant professor at University of Wyoming. His research activities include first-principles calculations, molecular simulations, and multiscale modeling of a variety of nanostructured materials. His recent interest is focused on the mechanical, electronic, and spin properties of hybrid two-dimensional atomic monolayers. He is the author of over 30 publications that have been cited more than 1,600 times.